# The Tapered Gridded Estimator (TGE)

Somnath Bharadwaj

Indian Institute of Technology, Kharagpur

# Major Contributors

Asif Elahi
PH.D. Student
IIT Kharagpur

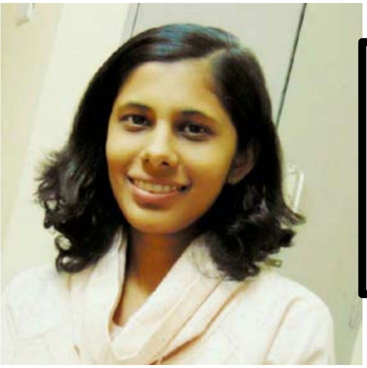

Sirjita Pal
PH.D. Student
(thesis submitted)
IIT Kharagpur

Samir Choudhuri
Ass. Prof.
IIT Madras

Ex-Ph.D. Student
IIT Kharagpur

Other Contributors

Abhik Ghosh, Sk. Saiyad Ali, Nirupam Roy

# Our Aim

Redshifted HI 21-cm
Brightness Temperature Fluctuations

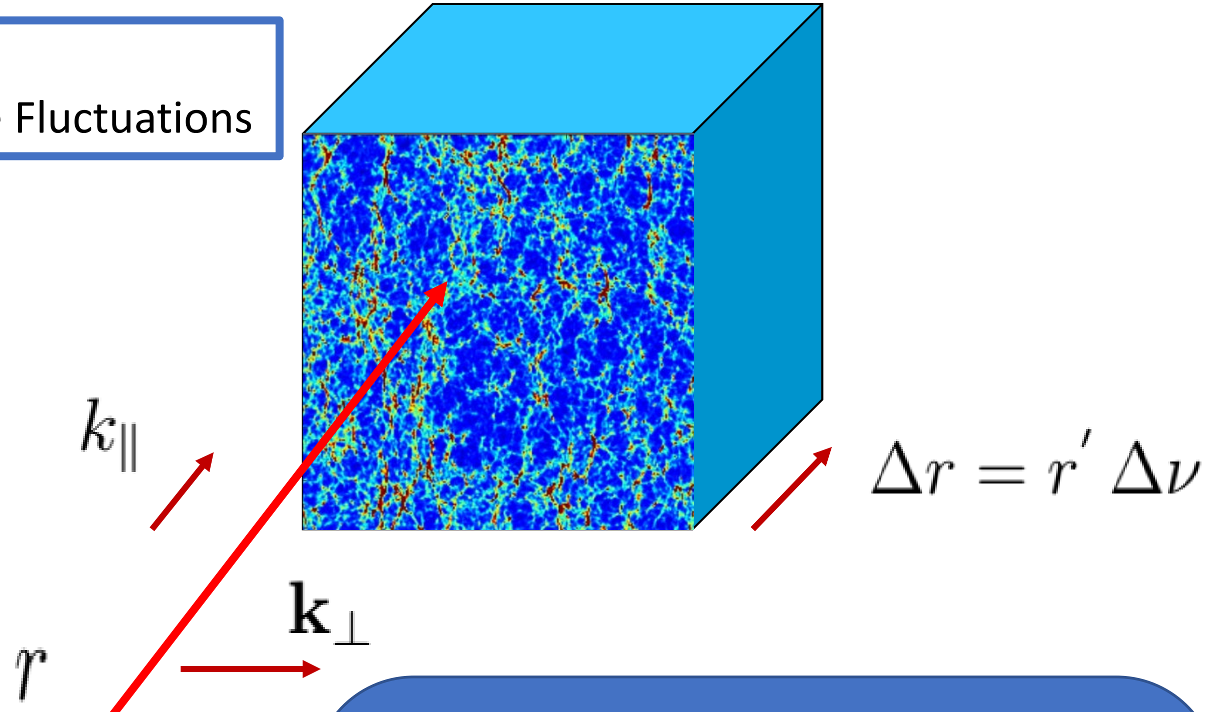


Radio Interferometric Array GMRT

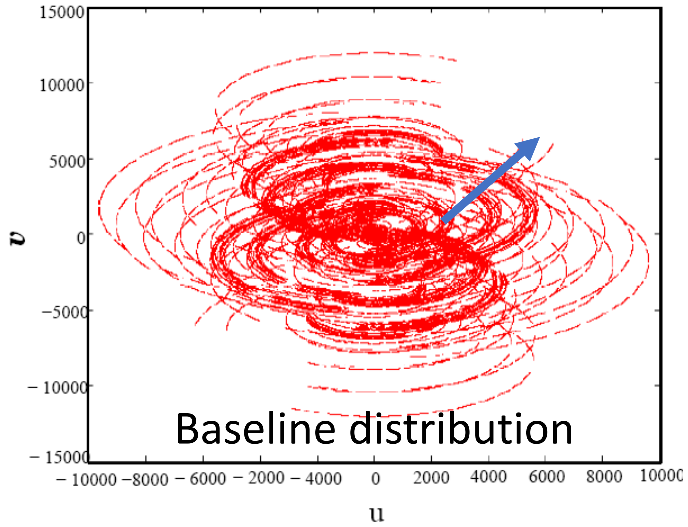


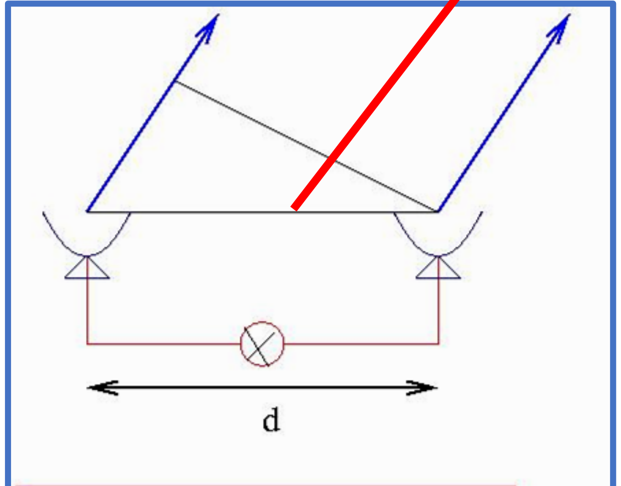


21-cm power spectrum $P(k_{\perp}, k_{\parallel})$

Visibility $\mathcal{V}(\mathbf{U}, \nu)$

# Visibility Correlation

$$\langle \mathcal{V}(\mathbf{U},\nu)\mathcal{V}(\mathbf{U},\nu+\Delta\nu)\rangle = \left[\frac{Q^2\theta_0^2}{2r^2}\right]\int_0^\infty dk_\parallel \; \cos(k_\parallel r' \, \Delta\nu)\, P(k_\perp, k_\parallel)$$

$$\mathbf{k}_\perp = \frac{2\pi\mathbf{U}}{r}$$

$$Q = 2k_B/\lambda^2$$ Conversion Factor

$$\theta_0 = 0.6\,\theta_{\rm HWHM}$$ of Primary Beam

Bharadwaj & Sethi, 2001

# Power Spectrum Estimation -2 Step

$$\langle \mathcal{V}(\mathbf{U},\nu)\mathcal{V}(\mathbf{U},\nu+\Delta\nu)\rangle = \left[\frac{\pi Q^2\theta_0^2}{2}\right] C_\ell(\Delta\nu)$$

$$\ell = 2\pi U$$

$$P(k_\perp, k_\parallel) = r^2 r' \int_{-\infty}^{\infty} d(\Delta\nu)\, e^{-ik_\parallel r'\Delta\nu}\, C_\ell(\Delta\nu)$$

$$k_\perp = \ell/r$$

Datta et al. 2007

# Multi-frequency Angular Power Spectrum

MAPS

$$\delta T_{\rm b}(\hat{\boldsymbol{n}}, \nu) = \sum_{\ell, m} a_{\ell {\rm m}}(\nu)\, Y_\ell^{\rm m}(\hat{\boldsymbol{n}})$$

$$C_\ell(\nu_a, \nu_b) = \langle a_{\ell {\rm m}}(\nu_a)\, a^*_{\ell {\rm m}}(\nu_b) \rangle$$

$$C_\ell(\Delta\nu) \text{ where } \Delta\nu = | \nu_b - \nu_a |$$

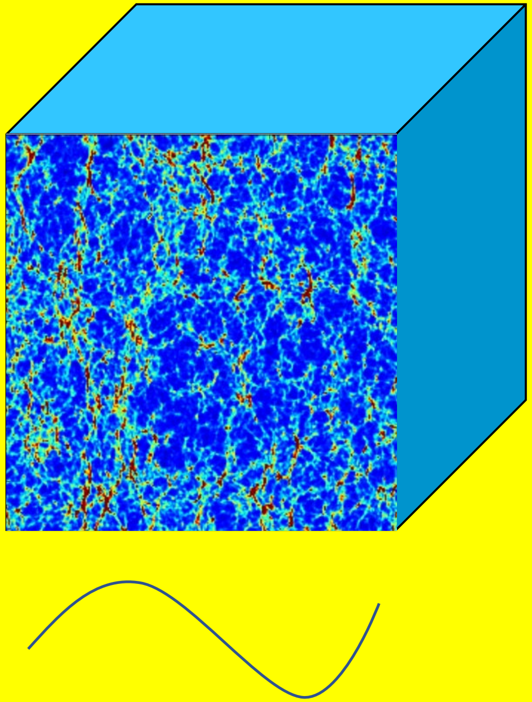

Fourier Modes in
Flat Sky Approximation

# Tapered Gridded

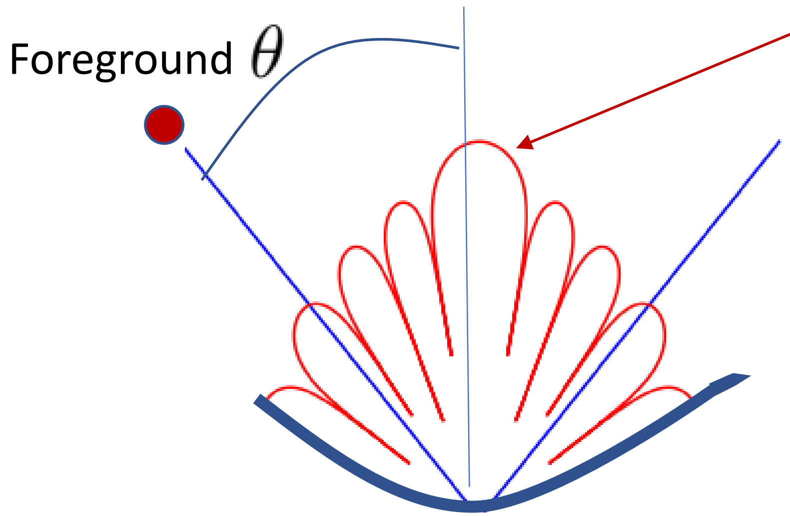


**Primary Beam Pattern**

$$\mathcal{A}(\theta) \approx e^{-\theta^2/\theta_0^2}$$

**Tapering Window**

$$\mathcal{W}(\theta) = e^{-\theta^2/\theta_w^2}$$

$$\theta_w = f\theta_0$$

Tapering parameter $f \leq 1$

smaller $f$ - more tapering

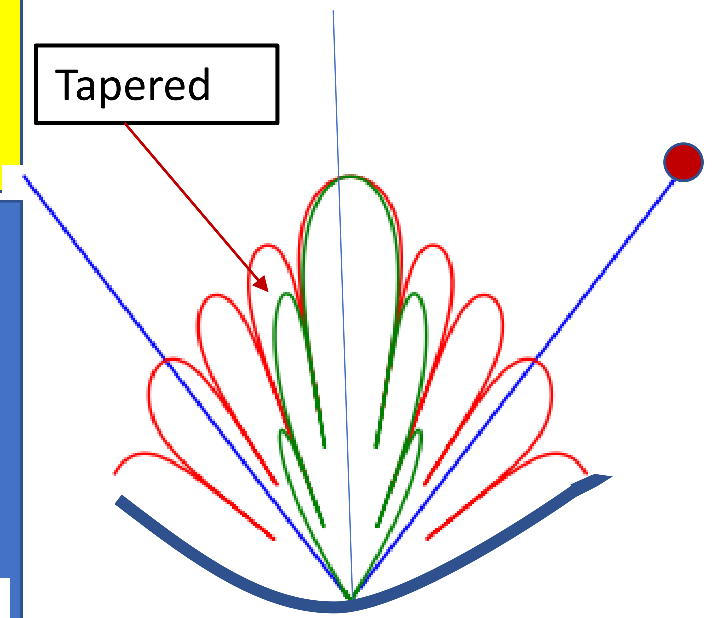


**Convolution**

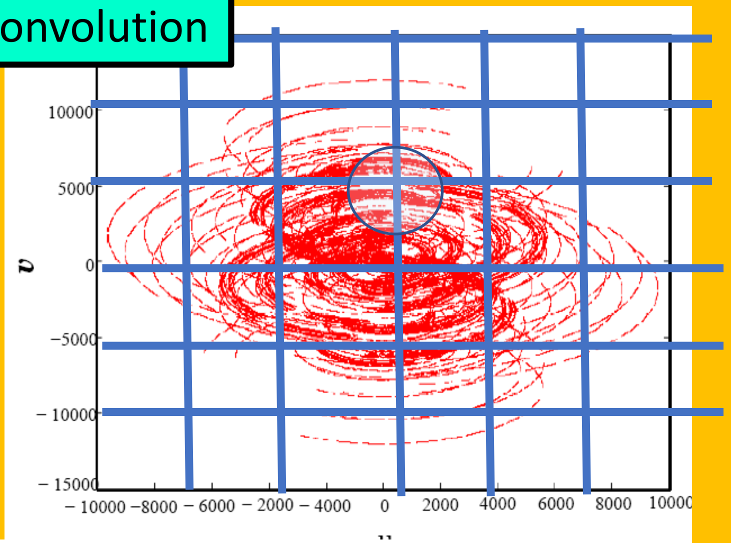


$$\mathcal{V}_{cg}(\nu_a) = \sum_i \tilde{w}(\mathbf{U}_g - \mathbf{U}_i)\, \mathcal{V}_i(\nu_a)\, F_i(\nu_a).$$

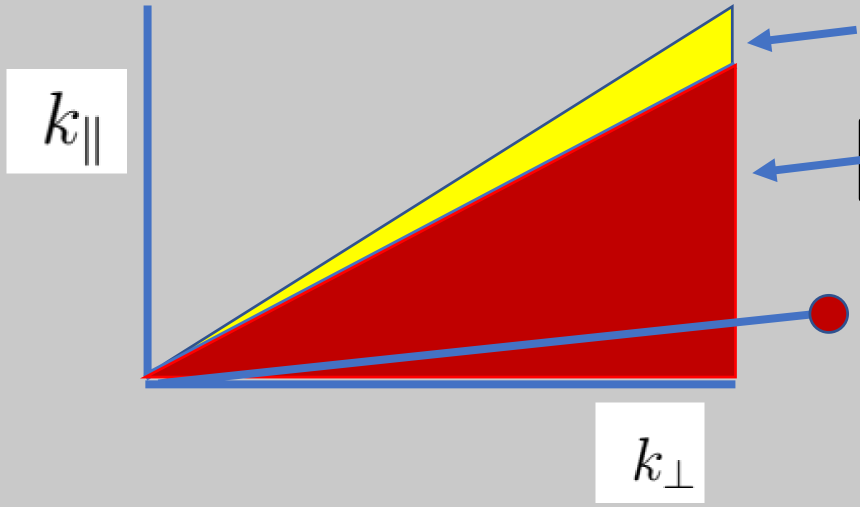


Foreground Leakage

Foreground Wedge

$$k_{\parallel} = \left[\frac{r\,\sin(\theta)}{r'\nu_c}\right] k_{\perp}$$

# Tapered Gridded Estimator - TGE

$$\hat{E}_g(\nu_a,\nu_b) = M_g^{-1}(\nu_a,\nu_b)\mathcal{R}e\Big[\mathcal{V}_{cg}(\nu_a)\mathcal{V}_{cg}^*(\nu_b) - \sum_i F_i(\nu_a)F_i(\nu_b) \mid \tilde{w}(\mathbf{U}_g - \mathbf{U}_i) \mid^2 \mathcal{V}_i(\nu_a)\mathcal{V}_i^*(\nu_b)\Big]$$

Visibility Correlation

Subtract Noise Bias due to self correlation

$M_g(\nu_a,\nu_b)$ is a normalization constant

Used Simulations with Unit MPAS → $C_\ell(\nu_a,\nu_b) = 1$ → $[\mathcal{V}_i(\nu_a)]_{\rm UMAPS}$

$$M_g(\nu_a,\nu_b) = \mathcal{R}e\Big[\mathcal{V}_{cg}(\nu_a)\mathcal{V}_{cg}^*(\nu_b) - \sum_i F_i(\nu_a)F_i(\nu_b) \mid \tilde{w}(\mathbf{U}_g - \mathbf{U}_i) \mid^2 \mathcal{V}_i(\nu_a)\mathcal{V}_i^*(\nu_b)\Big]_{\rm UMAPS}$$

Unbiased Estimator

$$\langle \hat{E}_g(\nu_a,\nu_b)\rangle = C_{\ell_g}(\nu_a,\nu_b)$$

# Binning

$$C_\ell(\nu_a, \nu_b) \longrightarrow C_\ell(\Delta\nu)$$

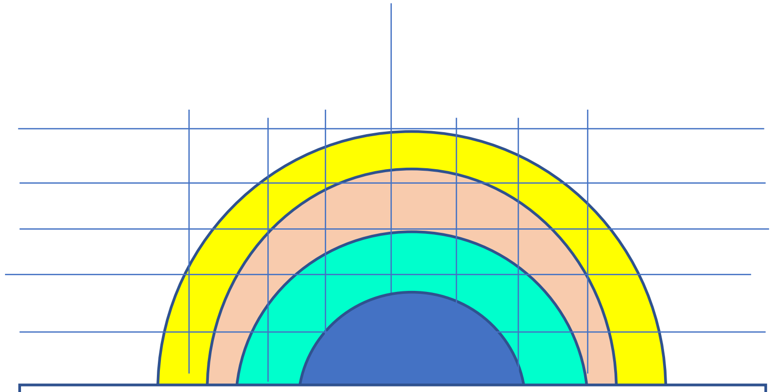

Annular bins

# Power Spectrum

Fourier transform

$$C_\ell(n\,\Delta\nu_c) = \sum_m \mathbf{A}_{nm}\,\bar{P}(k_\perp, k_{\parallel m}) + [\mathrm{Noise}]_n$$

Maximum Likelihood

$$\bar{P}(k_\perp, k_{\parallel m}) = \sum_n \{[\mathbf{A}^\dagger \mathbf{N}^{-1} \mathbf{A}]^{-1} \mathbf{A}^\dagger \mathbf{N}^{-1}\}_{mn} \{\mathcal{W}_{\mathrm{BN}}(n\Delta\nu_c) C_\ell(n\Delta\nu_c)\}$$

window function $\mathcal{W}_{\mathrm{BN}}(n\Delta\nu_c)$ along the $\Delta\nu$

# Flagging

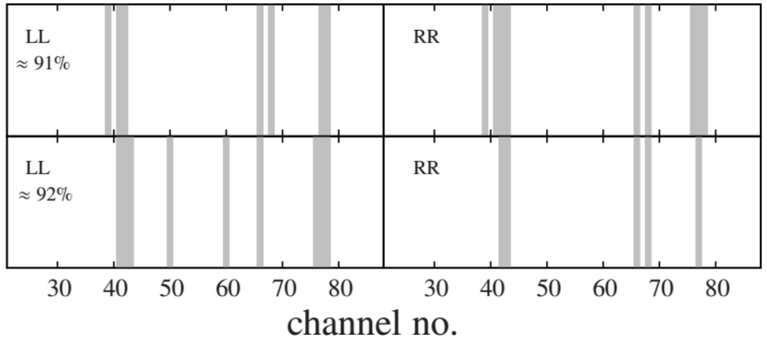


5.5 MHz

**Figure 1.** Unflagged frequency channels (shown in grey) for two randomly chosen baselines $U = 82\,\lambda$ (upper panels) and $2688\,\lambda$ (lower panels) for which respectively 91% and 92% of the channels are flagged. Stokes LL and RR are shown in the left and right panels respectively.

47 % of data flagged

# Validation

$$P^m(k) = (k/k_0)^n \text{ mK}^2 \text{ Mpc}^3$$

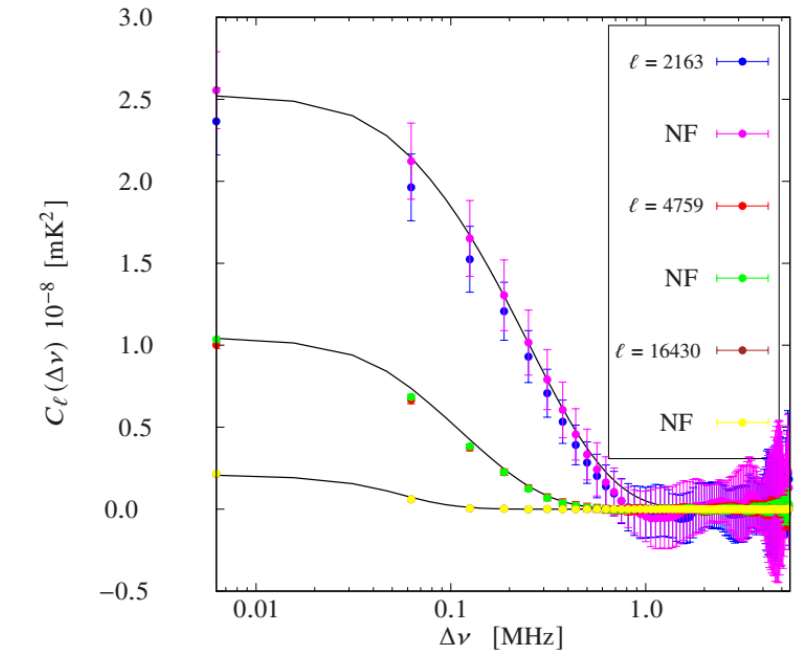


$$k_0 = (1.1)^{-1/2} \text{ Mpc}^{-1}$$

$$n = -2.$$

Simulations

f-=0.6

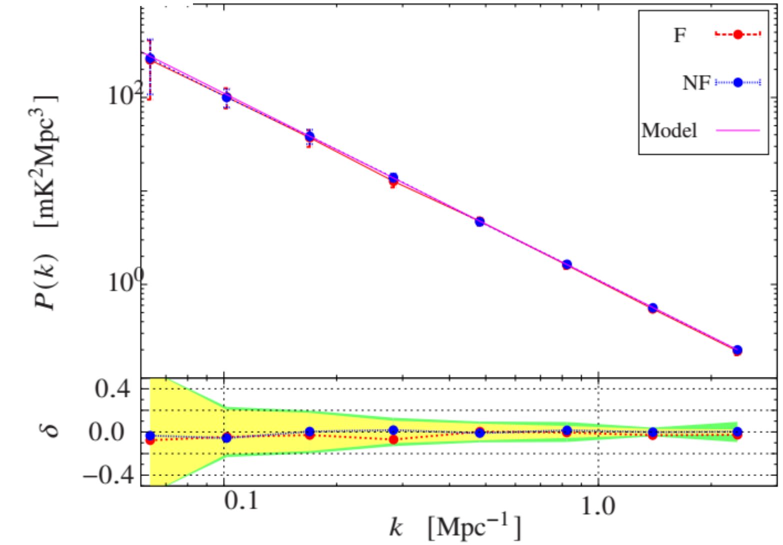


Pal, S. et al. 2021

# The Tracking Tapered Gridded Estimator (TTGE) for the power spectrum from drift scan observations

Suman Chatterjee[1], Somnath Bharadwaj[2], Samir Choudhuri[3,4], Shiv Sethi[5] and Akash Kumar Patwa[5]

2023, MNRAS

# Tracking Tapered Gridded Estimator for the 21-cm power spectrum using MWA drift scan observations I: Formalism and preliminary results

Suman Chatterjee[1], Khandakar Md Asif Elahi[2], Somnath Bharadwaj[2], Shouvik Sarkar[3], Samir Choudhuri[3], Shiv Sethi[4] and Akash Kumar Patwa[4]

In Preparation

# MWA Drift Scan Observations

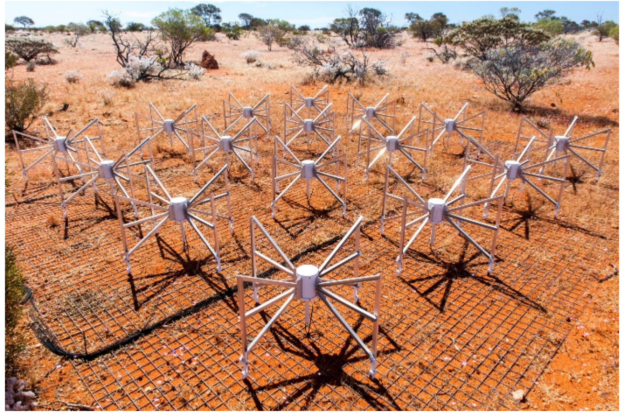

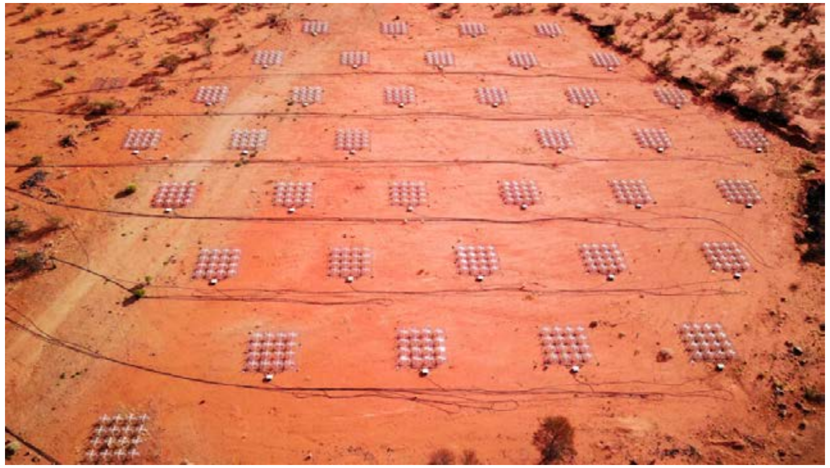

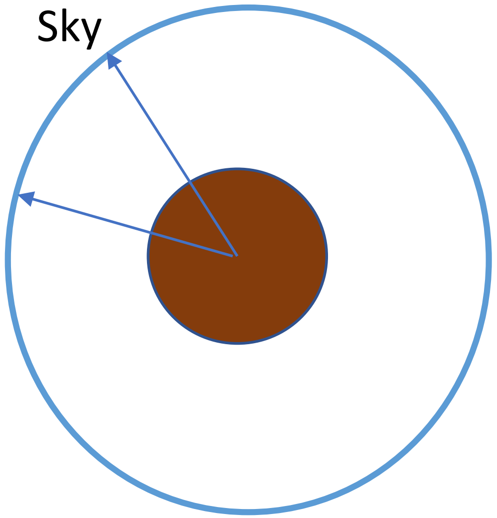


Marchison Widefield Array MWA

Drift Scan Observations

Tracking Center

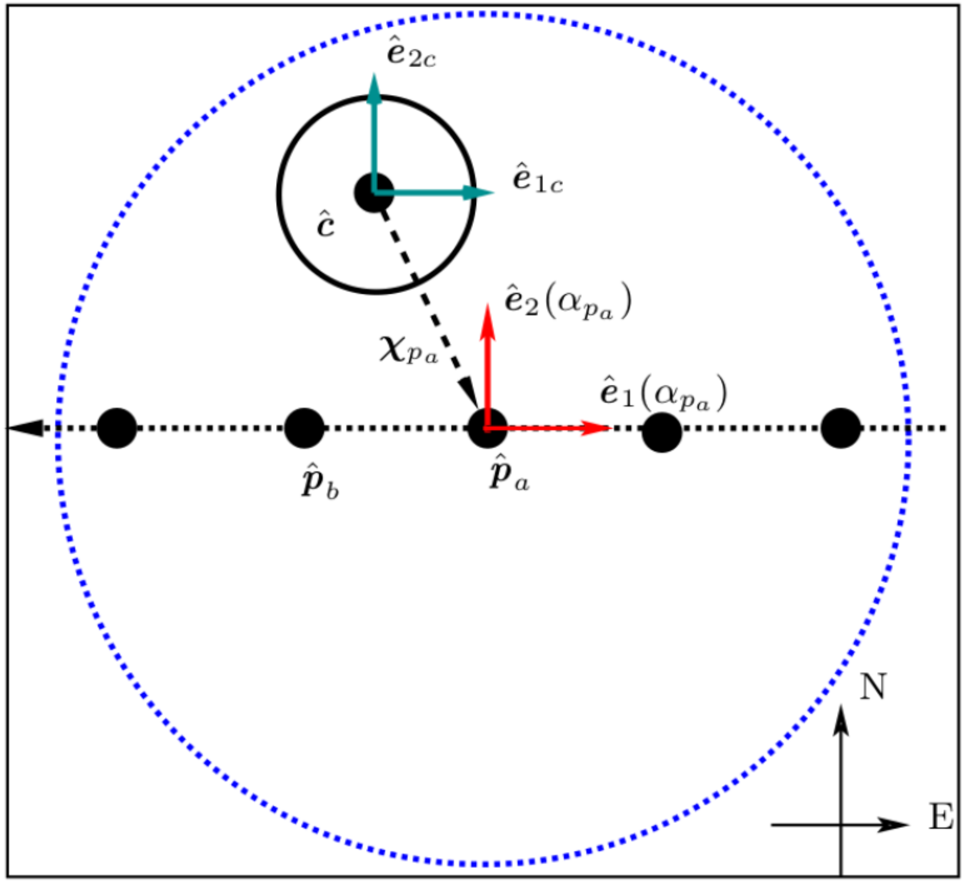


**Figure 1.** This shows a schematic diagram of drift scan observations. Filled circles (marked by $\hat{p}_a, \hat{p}_b, \ldots$) are the different pointing direction of the telescope, and the dashed circle represents the FWHM of the MWA primary beam when the telescope is pointing towards $\hat{p}_a$ for which the basis vectors $\hat{e}_1(\alpha_{p_a})$ and $\hat{e}_2(\alpha_{p_a})$ are also shown. $\hat{c}$ refers to the tracking center for which $\hat{e}_{1c}$ and $\hat{e}_{2c}$ are the corresponding basis vectors. The solid circle around $\hat{c}$ show the FWHM of the tapering window, and $\chi_{p_a} = \hat{p}_a - \hat{c}$.

# Tracking TGE

$$\mathcal{V}_{cg}(\nu) = \sum_p s_p \sum_n \tilde{w}(\boldsymbol{U}_g - \boldsymbol{U}_n) e^{2\pi i \boldsymbol{U}_n \cdot \chi_p} \mathcal{V}(\alpha_p, \boldsymbol{U}_n, \nu)$$

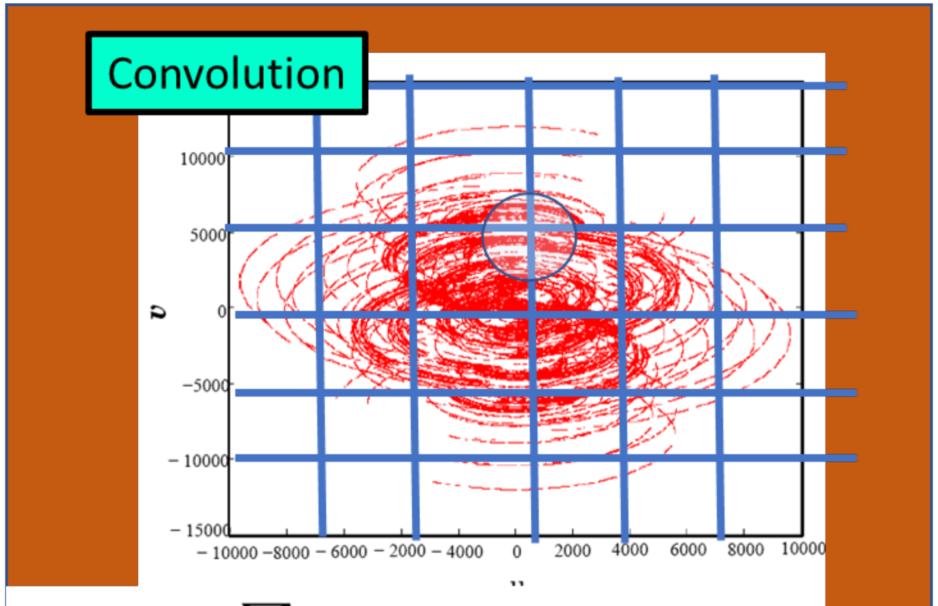


$$\mathcal{V}_{cg}(\nu_a) = \sum_i \tilde{w}(\mathbf{U}_g - \mathbf{U}_i)\, \mathcal{V}_i(\nu_a)\, F_i(\nu_a).$$

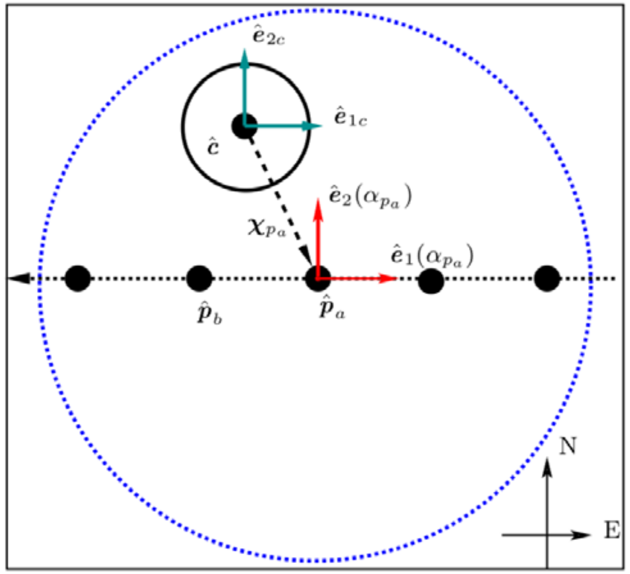


**Figure 1.** This shows a schematic diagram of drift scan observations. Filled circles (marked by $\hat{p}_a, \hat{p}_b, \ldots$) are the different pointing direction of the telescope, and the dashed circle represents the FWHM of the MWA primary beam when the telescope is pointing towards $\hat{p}_a$ for which the basis vectors $\hat{e}_1(\alpha_{p_a})$ and $\hat{e}_2(\alpha_{p_a})$ are also shown. $\hat{c}$ refers to the tracking center for which $\hat{e}_{1c}$ and $\hat{e}_{2c}$ are the corresponding basis vectors. The solid circle around $\hat{c}$ show the FWHM of the tapering window, and $\chi_{p_a} = \hat{p}_a - \hat{c}$.

# MWA Drift Scan Observations

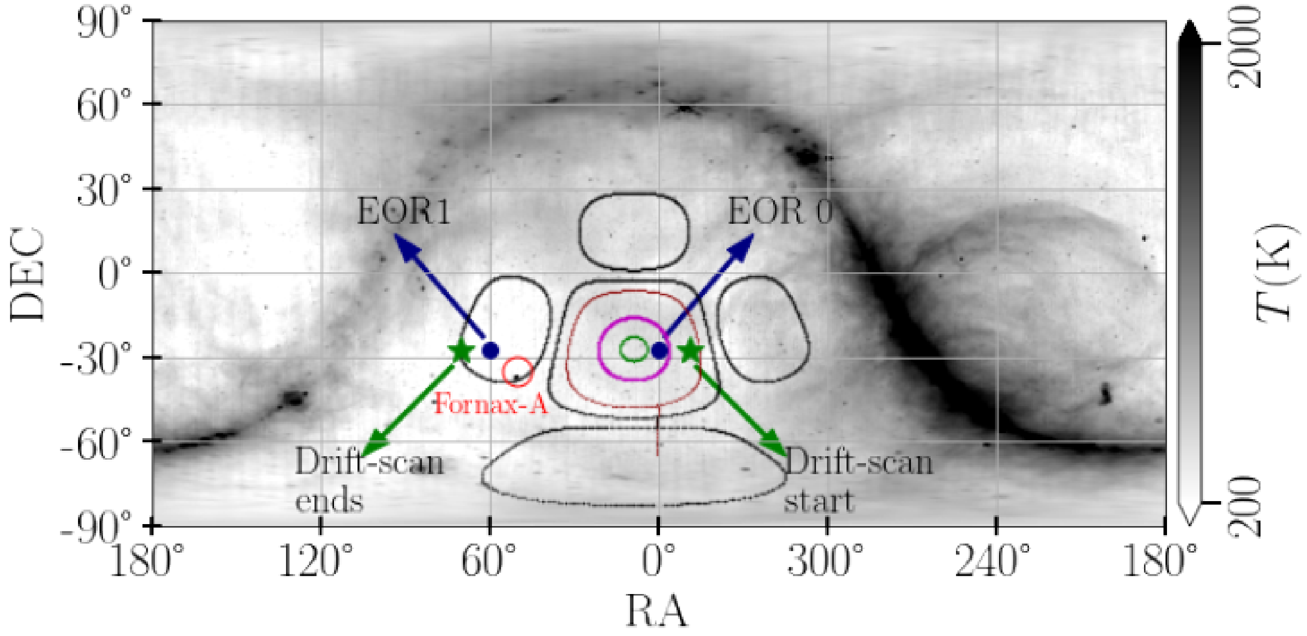


**Figure 1.** This shows the 408 MHz Haslam map (Haslam et al. 1982) scaled to 154 MHz assuming the brightness temperature spectral index $\alpha = -2.52$ (Rogers & Bowman 2008). The iso-contours in green, magenta, red and black show the MWA primary beam at values 0.9, 0.5, 0.05 and 0.005 respectively for a pointing center at $(6.1°, -26.7°)$ which corresponds to the data analysed here. The scan starts roughly at the location of the '$\star$' on the right (RA=349°) and lasts until the '$\star$' on the left (RA=70.3°). Blue filled circles mark the fields EoR $0(0°, -26.7°)$ and EoR $1(60°, -26.7°)$. The red circle shows the position of Fornax A.

# Flagging

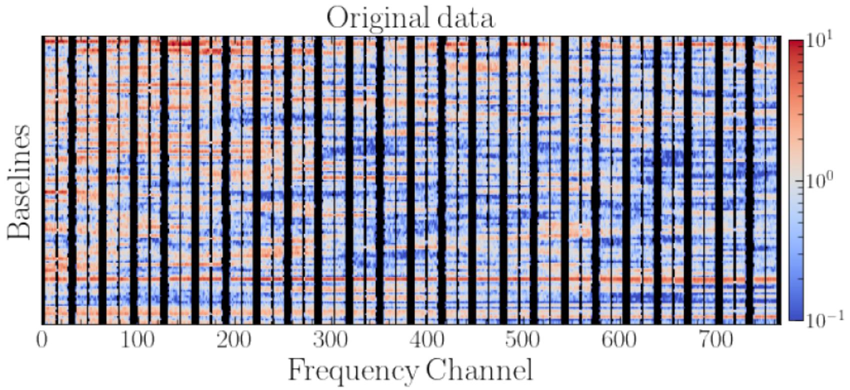


**Figure 2.** This shows the periodic channel flagging in the observed MWA visibility data. The entire frequency bandwidth is divided into 24 coarse bands of 32 channels or 1.28 MHz width each. The colors here shows arbitrarily normalised visibility amplitudes, and the black vertical lines indicate the flagged channels.

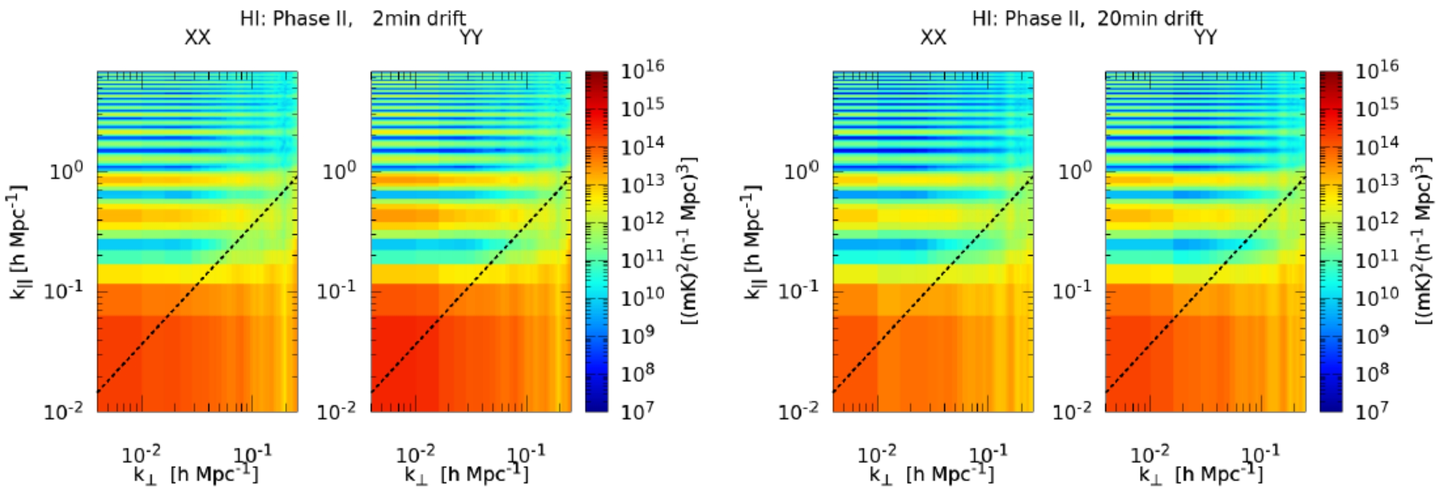


**Figure 7.** Two-dimensional power spectra are displayed for two fixed periods (2 and 20 minutes) of drift scans. The diagonal black line (plotted using the main lobe of MWA's primary beam) separate the EoR window (the region above the line) from the foreground-dominated modes.

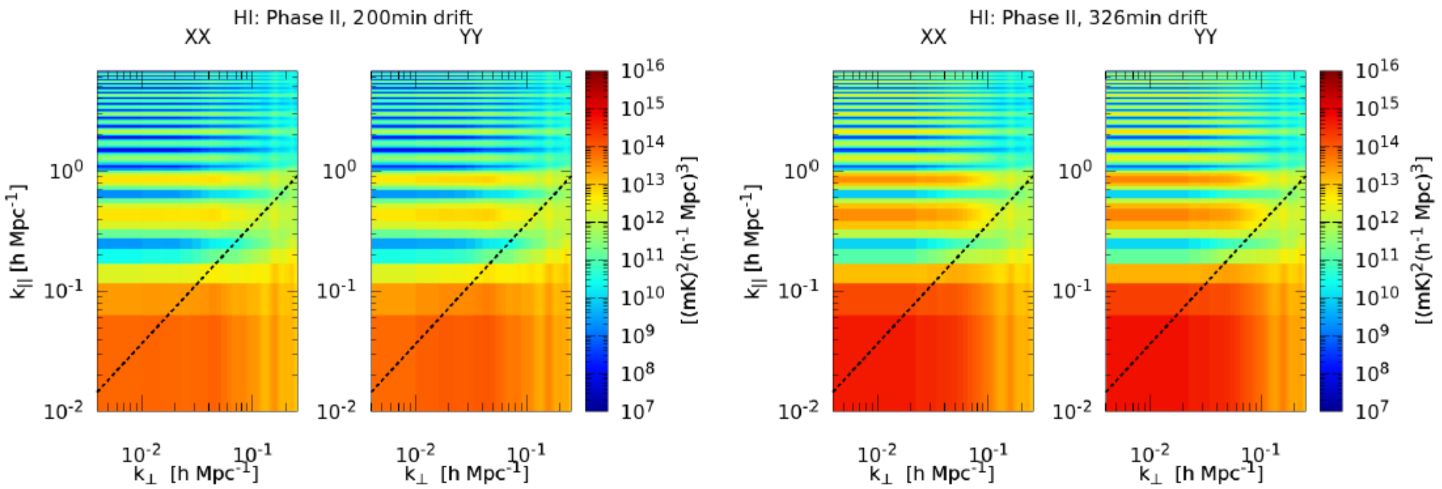


**Figure 8.** The 10-night combined data are displayed for 200 minutes and 326 minutes of drift scan.

Patwa, A. et. al. 2021

# Simulated MAPS

$$P^m(k) = (k/k_0 = 1)^{-1}(\mathrm{K}^2\mathrm{Mpc}^3)$$

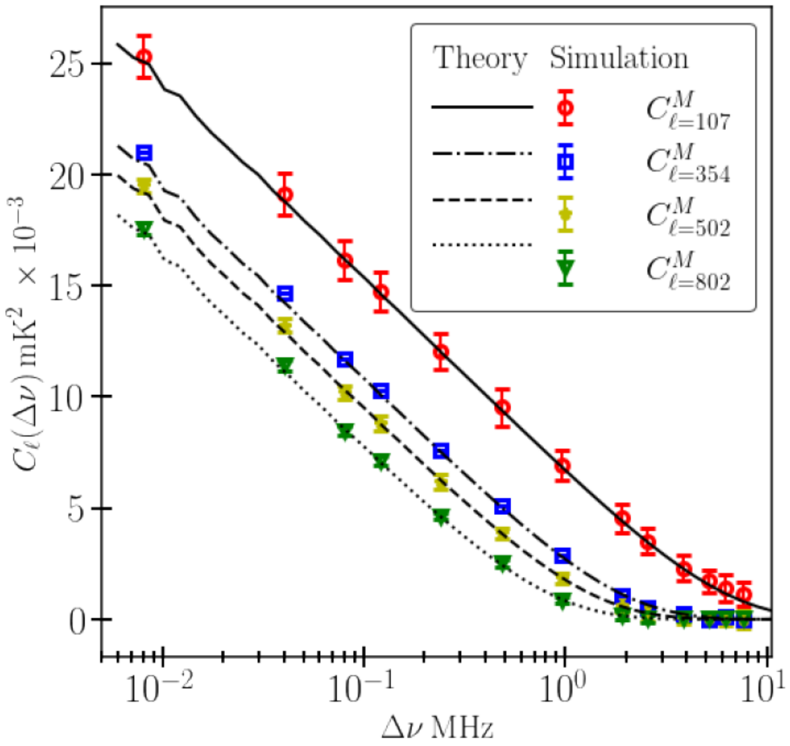


**Figure 3.** This shows $C_\ell(\Delta\nu)$ as a function of $\Delta\nu$ for four values of $\ell$. The data points with $1\sigma$ error bars are estimated from 20 realizations of the all-sky simulations. The lines show the theoretical predictions calculated using the input model power spectrum $P^m(k)$ in equation (16). The $\Delta\nu = 0$ points have been slightly shifted for the convenience of plotting on a logarithmic scale.

# Validation

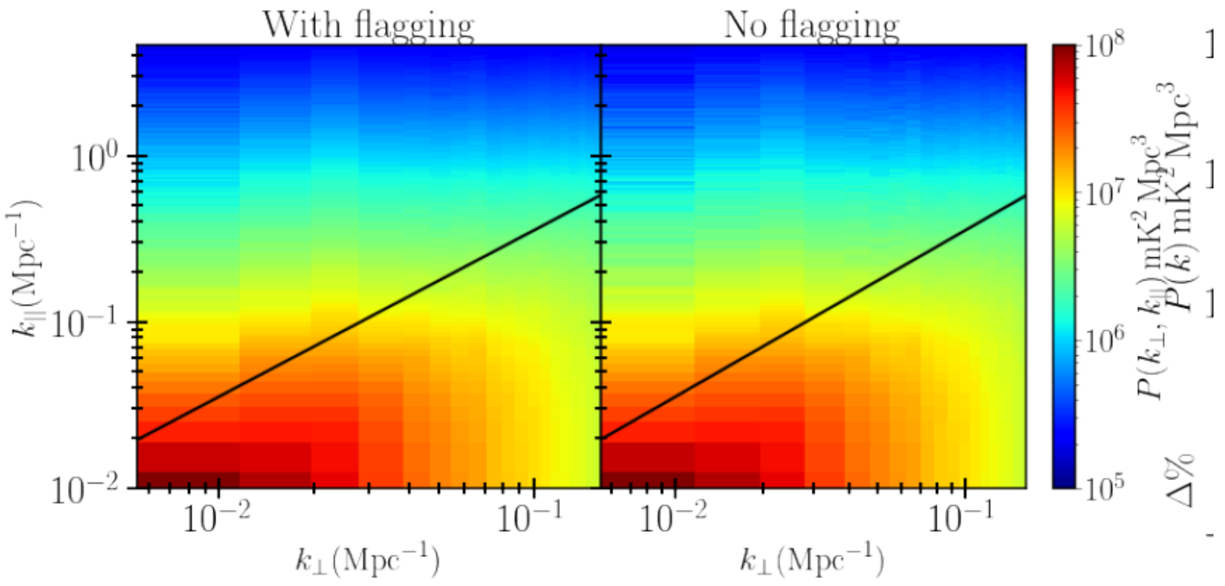


**Figure 4.** Left panel shows the simulated cylindrical power spectrum $P(k_\perp, k_\parallel)$ estimated from simulations with MWA coarse channel flagging. For comparison we show the $P(k_\perp, k_\parallel)$ estimated from simulations without coarse channel flagging in the right panel. We do not notice any significant differences.

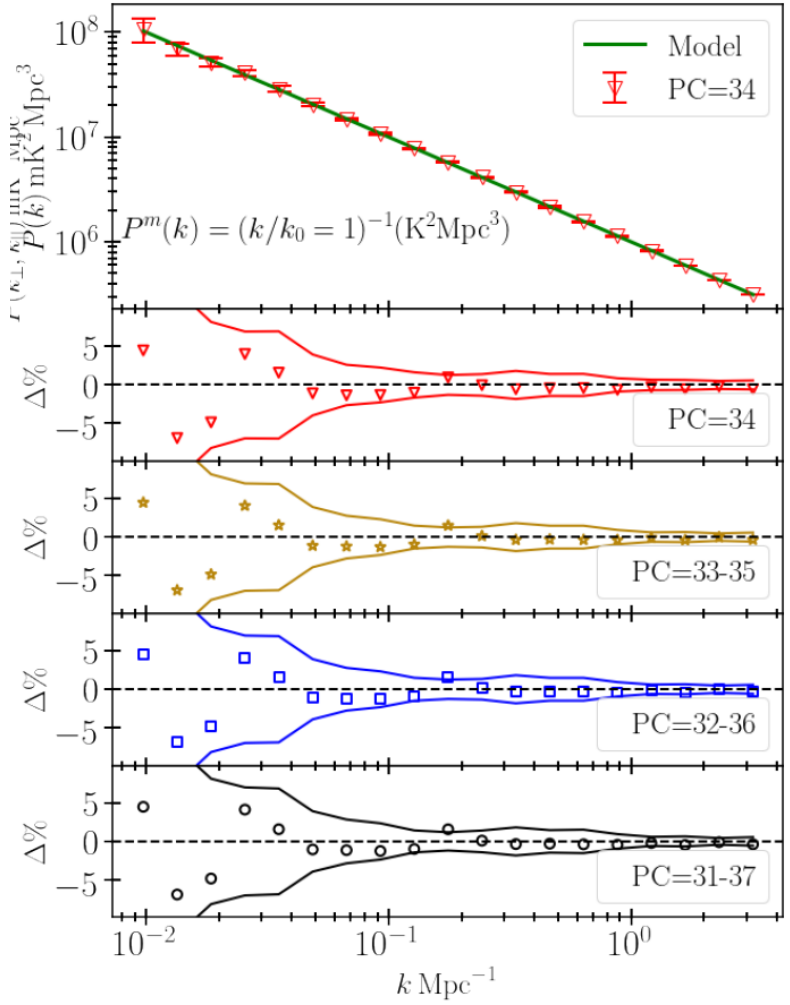


**Figure 5.** The upper panel shows the estimated spherically binned power spectrum $P(k)$ and $1-\sigma$ error bars for simulations for PC=34 with no noise and coarse channel flagging. For comparison, the input model $P^m(k)$ is also shown by the solid line. The lower panels show the percentage error $\Delta = [P(k) - P^m(k)]/P^m(k)$ (data points) and the relative statistical fluctuation $\sigma/P^m(k) \times 100\%$ (between the solid lines). The four lower panels consider situations for combining different PCs mentioned in the figure legends.

# Single Pointing PC=34

$$X = \frac{P(k_\perp, k_\parallel)}{\delta P_N(k_\perp, k_\parallel)}$$

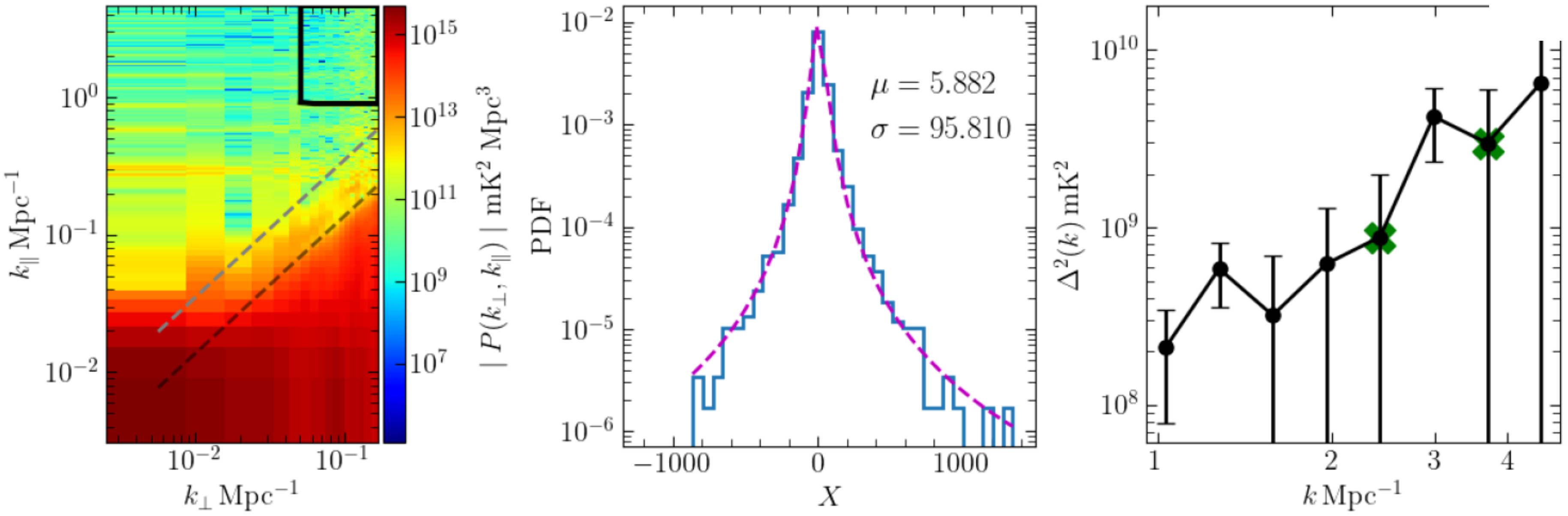


**Figure 9.** The left panel shows the cylindrical PS $|\,P(k_\perp, k_\parallel)\,|$. The grey and black dashed lines show the theoretically predicted boundary of foreground contamination expected from a monochromatic source located at the horizon and the FWHM of the telescope's PB, respectively. The region inside the black rectangle is used to constrain the 21-cm signal. The middle panel shows the histogram of the quantity $X = P(k_\perp, k_\parallel)/\delta P_N(k_\perp, k_\parallel)$ considering the modes inside the rectangle. The right panel shows $|\,\Delta^2(k)\,|$ the absolute values of the mean squared brightness temperature fluctuations and the corresponding $2\sigma$ error bars. The negative values of $\Delta^2(k)$ are marked with a cross.

brightness temperature fluctuations. The tightest upper limit is found to be $\Delta^2(k) < (1.85 \times 10^4)^2\,\mathrm{mK}^2$ at the first $k$-bin $k = 1\,\mathrm{Mpc}^{-1}$.

# MAPS

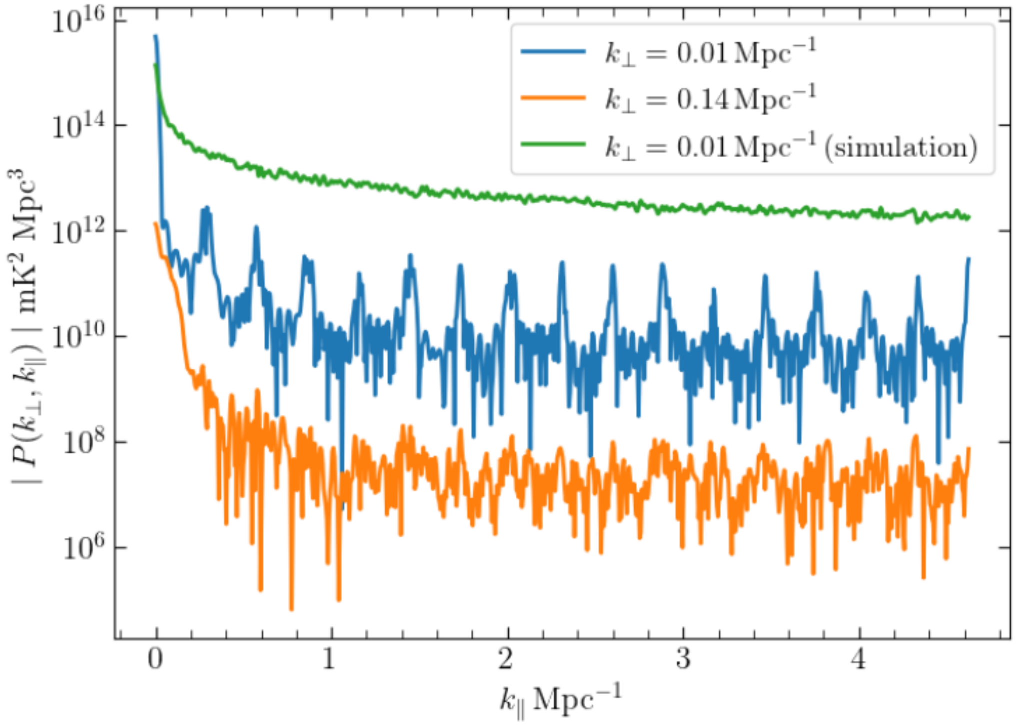


**Figure 10.** This figure shows $\mid P(k_\perp, k_\parallel) \mid$ as a function of $k_\parallel$ for two fixed values of $k_\perp$. The blue and orange curves are from the observed data, and the green curve is from the simulated data. The curve corresponding to $k_\perp = 0.13\,\mathrm{Mpc}^{-1}$ has been divided by a factor of $10^3$, and the curve showing the simulated data has been multiplied by $10^7$ for better visualization.

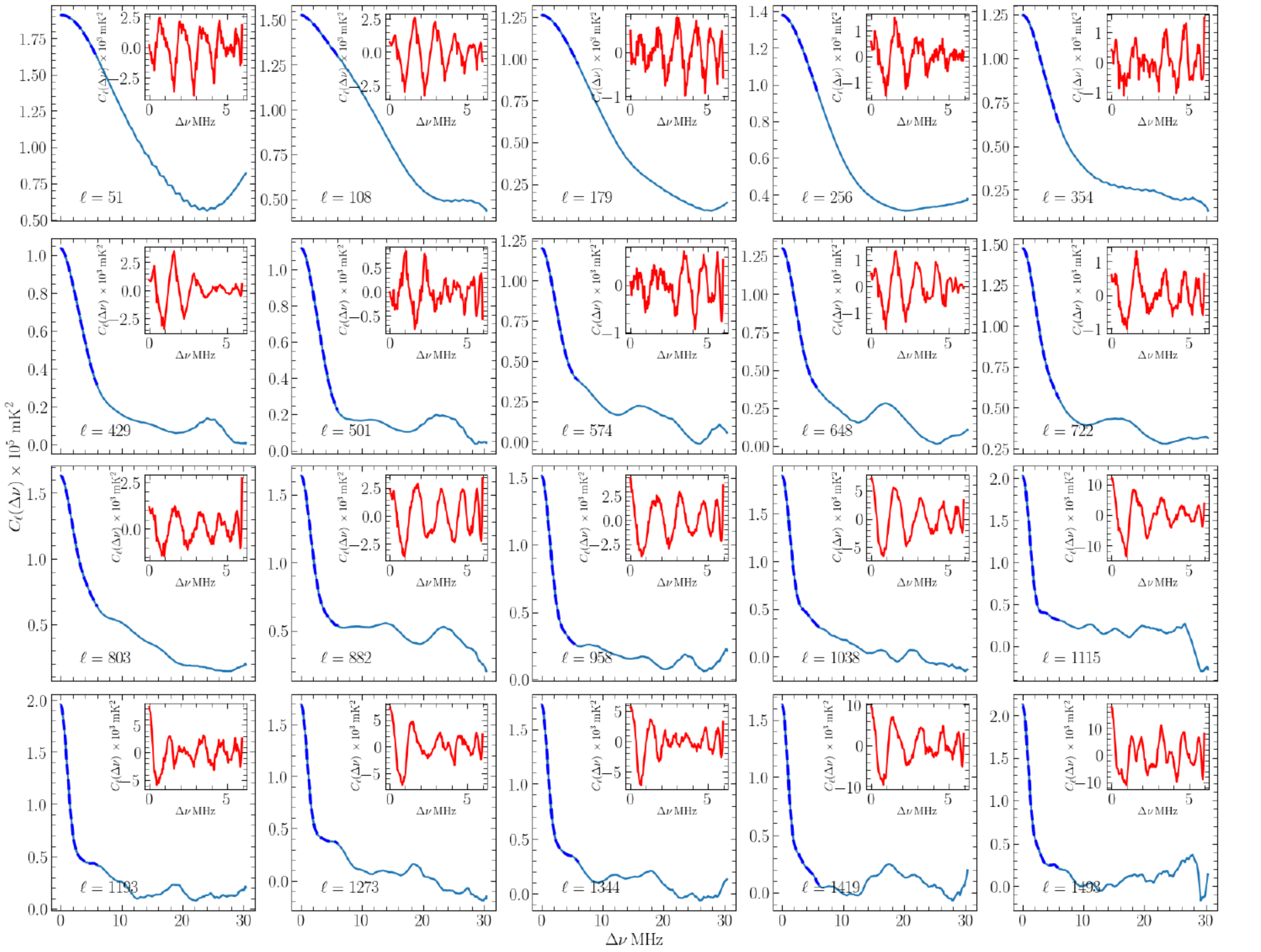


**Figure A1.** This figure shows $C_\ell(\Delta\nu)$ for the annotated $\ell$ values. The blue dashed curves show a polynomial fit on the range $\Delta\nu < 6$ MHz. The polynomial fit is subtracted from the measured $C_\ell(\Delta\nu)$, and the residual $C_\ell(\Delta\nu)$ are shown in the insets (red).

# MAPS

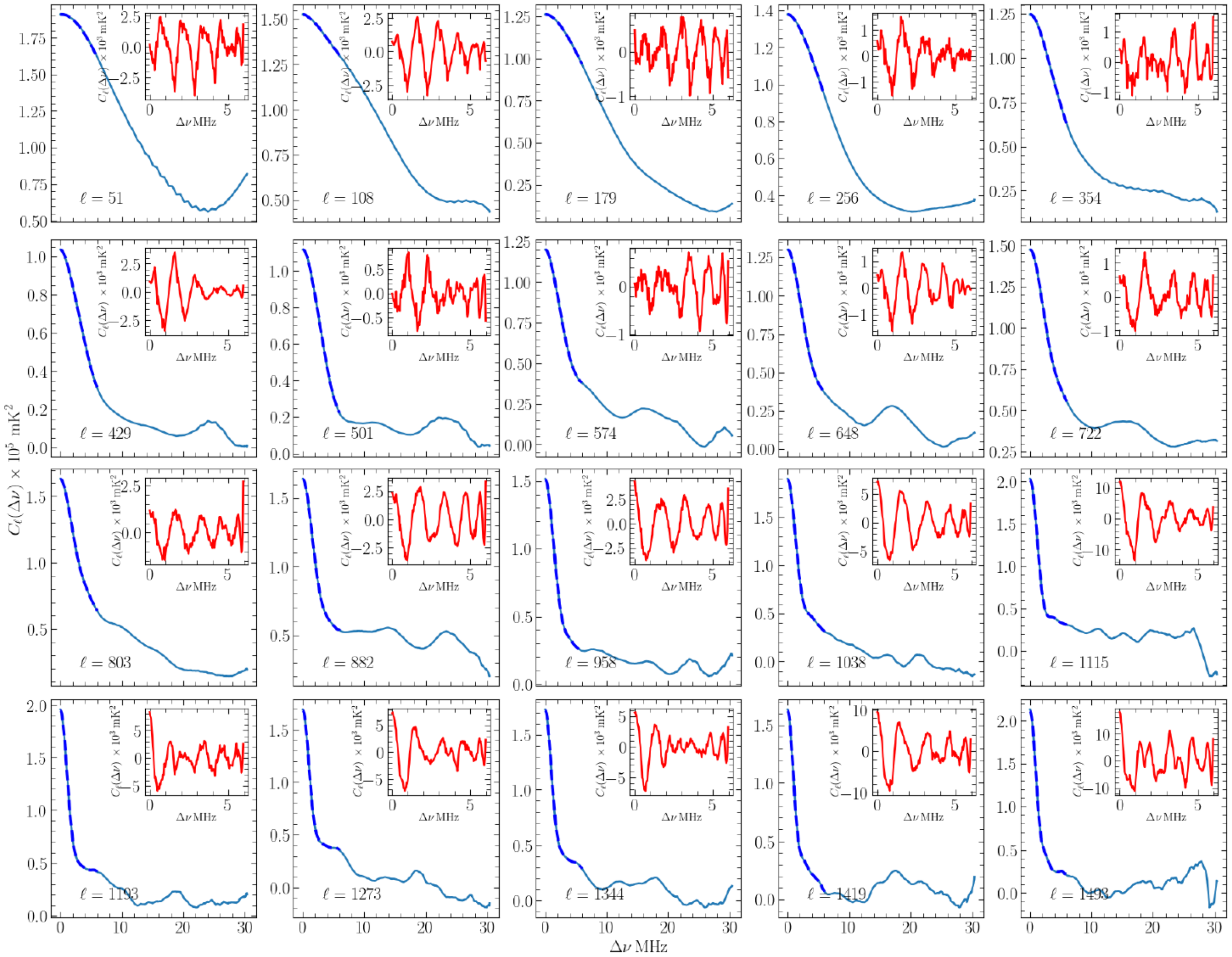


**Figure A1.** This figure shows $C_\ell(\Delta\nu)$ for the annotated $\ell$ values. The blue dashed curves show a polynomial fit on the range $\Delta\nu < 6$ MHz. The polynomial fit is subtracted from the measured $C_\ell(\Delta\nu)$, and the residual $C_\ell(\Delta\nu)$ are shown in the insets (red).

# Summary

- Tapered Gridded Estimator – 2 steps
- MAPS -> PS
- Tapers Widefield and Sidelobe response
- Tracking Tapered Gridded Estimator
- MWA 154 MHz drift scan observations
- Can combine multiple pointings for a single tracking center
- Validated using simulated all-sky data
- Actual data shows some small artefacts – can we model and remove these?

Thank you

# MAPS

Oscillations go down as f is reduced

We have used noise only simulations to estimate the error bars.

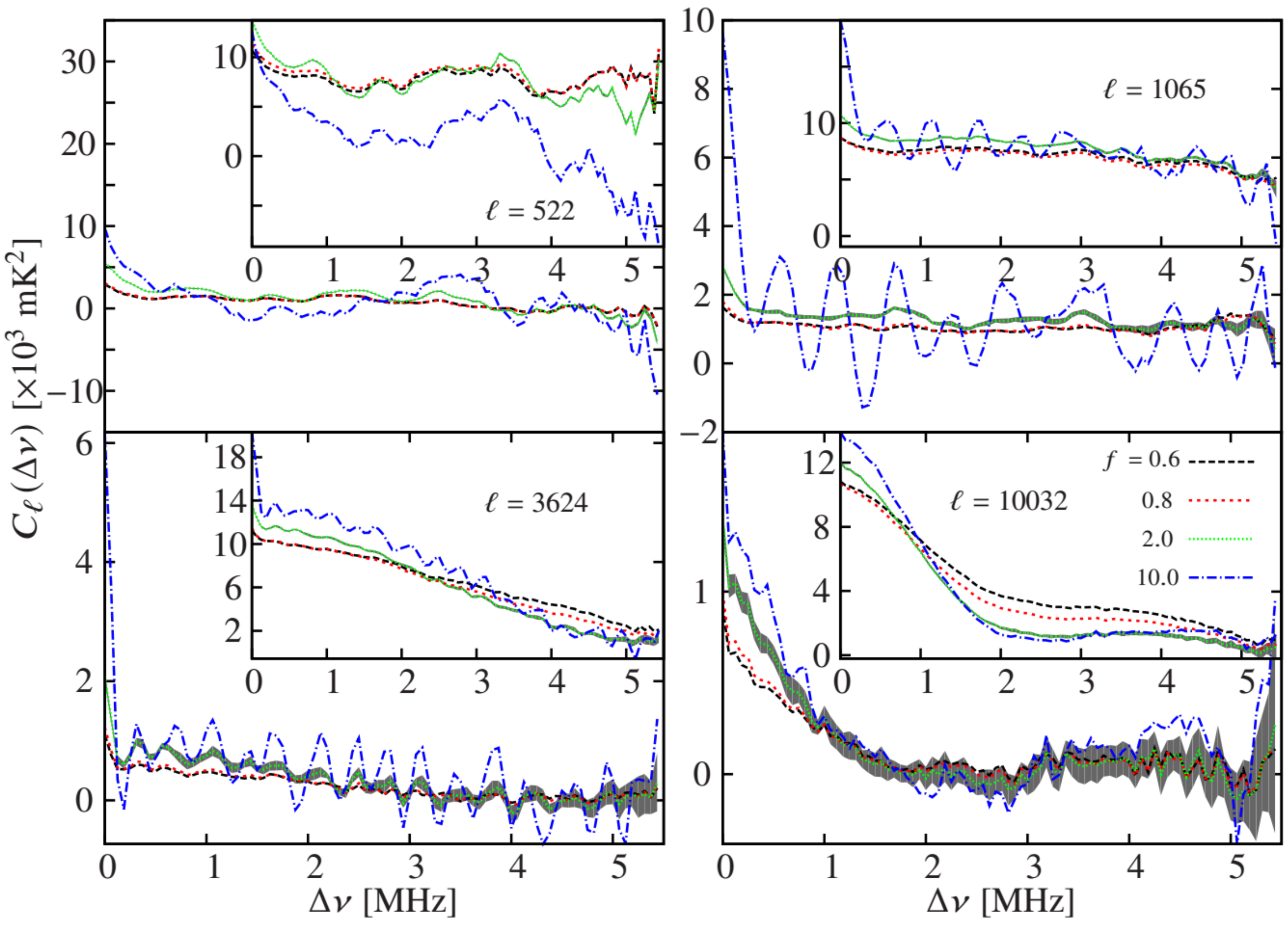


**Figure 4.** $C_\ell(\Delta\nu)$ as a function of $\Delta\nu$ after point source subtraction, with before point source subtraction shown as inset. The different panels correspond to different values of $\ell$, and the different lines correspond to different $f$ values as indicated in the legend. The black shaded regions for $f = 2.0$ displays the 10 $\sigma$ error bars due to the system noise only.

Pal, S. et al. 2021

# Cylindrical PS

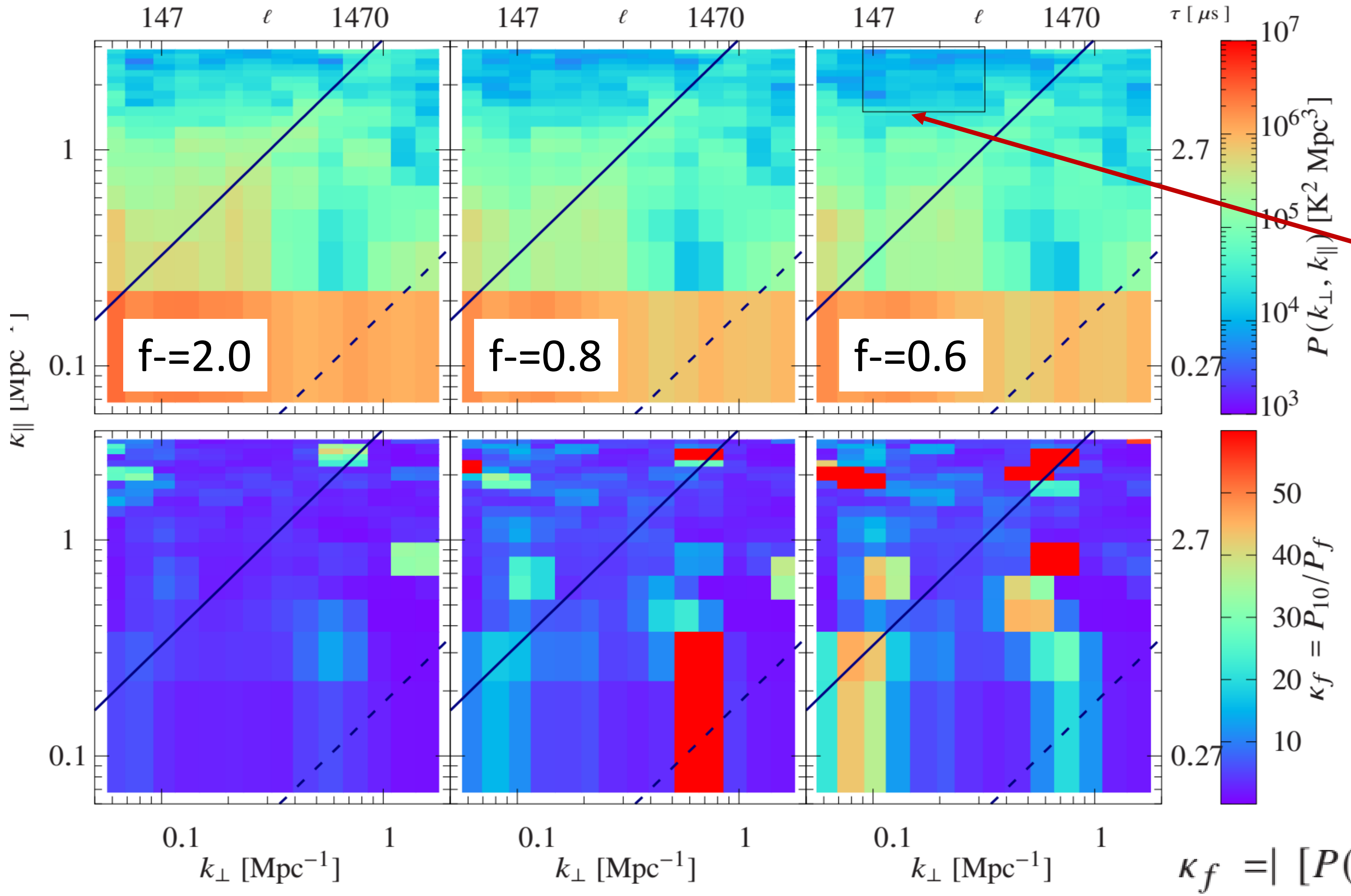


$$\kappa_f = | [P(k_{\perp}, k_{\parallel})]_{f=10.0} / [P(k_{\perp}, k_{\parallel})]_f$$

**Figure 9.** The upper row show the absolute value of the estimated cylindrical-binned power spectrum $P(k_{\perp}, k_{\parallel})$ after point source subtraction for different tapering $f = 2.0, 0.8, 0.6$ (left to right panels). The lower row show the corresponding $\kappa_f$ values. In all the cases, the solid and dashed lines respectively denote $[k_{\parallel}]_H$ and $[k_{\parallel}]_{\theta_1}$. Note that the $(k_{\perp}, k_{\parallel})$ modes enclosed within the rectangular area indicated in the upper right panel at $f = 0.6$, have been binned in the later part of the section to obtain the spherically binned averaged power spectrum $P(k)$.

Pal, S. et al. 2021

# Statistics

We need the statistics of $P(k_\perp, k_\parallel)$ in the clean region

Is it systematics, foregrounds or noise?

Noise level varies due to non-uniform baseline and channel coverage

We use simulations to estimate $\delta P_N(k_\perp, k_\parallel)$ the r.m.s. fluctuations expected from system noise alone

$$X = \frac{P(k_\perp, k_\parallel)}{\delta P_N(k_\perp, k_\parallel)}$$

Expected *zero* mean, unit variance

$$\mathrm{mean}(X) = 1.1 \text{ and } \sqrt{\mathrm{var}(X)} = 2.77$$

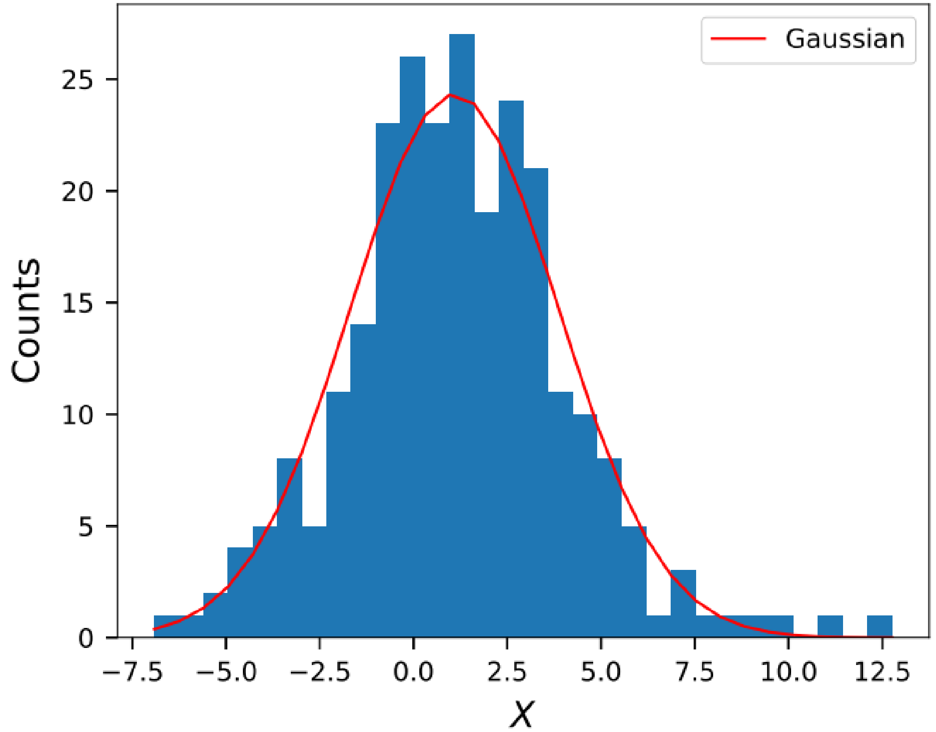


Actual noise more than expected

$$\delta P(k_\perp, k_\parallel) = \sqrt{\mathrm{var}(X)} \times \delta P_N(k_\perp, k_\parallel)$$

Small amount of foregrounds remains

$$(P(k_\perp, k_\parallel) \approx 0.4\, \delta P(k_\perp, k_\parallel))$$

# Results

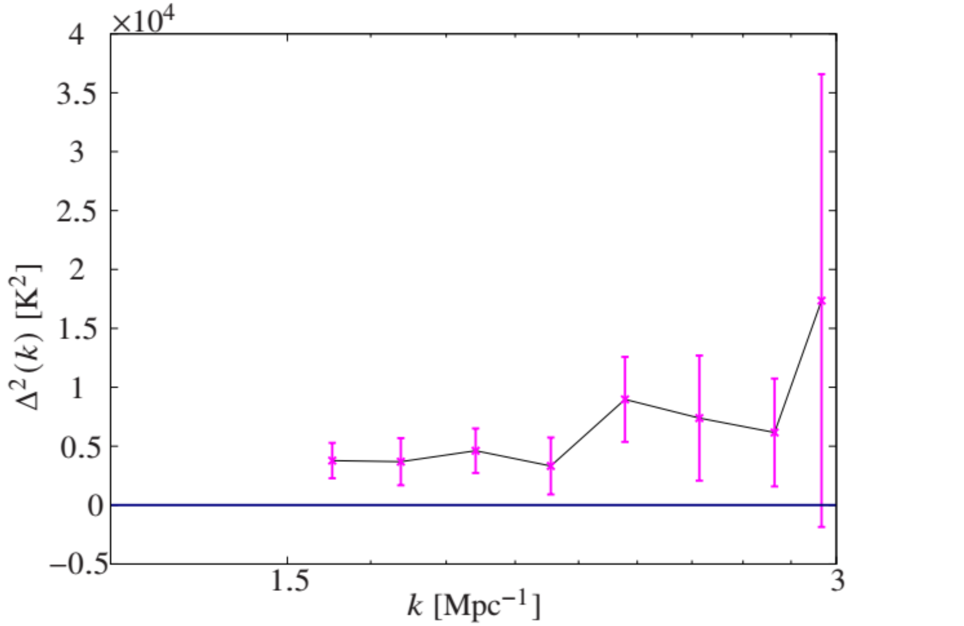


**Figure 12.** The mean square brightness temperature fluctuations $\Delta^2(k)$ shown as a function of $k$ along with 2 $\sigma$ error bars.

**Table 2.** Estimated spherically binned mean square brightness temperature fluctuations $\Delta^2(k)$ and statistical error predictions $\sigma$ for the same. The 2 $\sigma$ upper limits on $\Delta^2(k)$ ($\Delta^2_{UL}(k) = \Delta^2(k) + 2\,\sigma$) are listed corresponding to each $k$-bin.

| $k$ Mpc$^{-1}$ | $\Delta^2(k)$ K$^2$ $= k^3 P(k)/2\pi^2$ | $\sigma$ K$^2$ $= k^3 \delta P/2\pi^2$ | Upper limit, $\Delta^2_{UL}(k)$ (K)$^2$ [2$\sigma$] |
|---|---|---|---|
| 1.59 | $(61.47)^2$ | $(27.40)^2$ | $(72.66)^2$ |
| 1.73 | $(60.70)^2$ | $(31.61)^2$ | $(75.38)^2$ |
| 1.90 | $(67.96)^2$ | $(30.74)^2$ | $(80.68)^2$ |
| 2.09 | $(57.61)^2$ | $(34.75)^2$ | $(75.72)^2$ |
| 2.30 | $(94.74)^2$ | $(42.47)^2$ | $(112.17)^2$ |
| 2.52 | $(85.93)^2$ | $(51.53)^2$ | $(112.67)^2$ |
| 2.78 | $(78.50)^2$ | $(47.85)^2$ | $(103.64)^2$ |
| 2.94 | $(131.75)^2$ | $(98.00)^2$ | $(191.22)^2$ |

We have demonstrated the TGE

Tapers sky response

Works even with highly flagged data

Pal, S. et al. 2021

# uGMRT Band 3 Observations

| | |
|---|---|
| Working antennas | 28 |
| Central Frequency | 400 MHz |
| Number of Channels | 8192 |
| Channel width | 24.4 kHz |
| Bandwidth | 200 MHz |
| Total observation time | 25 h |
| Integration time | 2 s |
| Target field $(\alpha, \delta)_{2000}$ | $(16^h 10^m 1^s$, $+54°30'36'')$ |
| Galactic coordinates $(l, b)$ | 86.95°, +44.48° |

Removed Source: $> 100\mu$Jy

Chakraborty, A. et al. 2019

We analyse

24.4 MHz bandwidth uGMRT Band 3 data

centred at 432.8 MHz

aiming H I IM at $z = 2.28$

Total TGE (LL+RR) × (LL+RR)* Pal, S. et al. 2022

Cross TGE LL × RR* + cc. Elahi, A. 2023

Cross TGE + FG Removal Elahi, A. 2023

Delay Spectrum + CLEAN Chakraborty, A. et al. 2021

# MAPS

- Cross is significant improvement over Total
- Foregrounds are possibly polarised
- Calibrations errors in the two polarisations may be partially uncorrelated

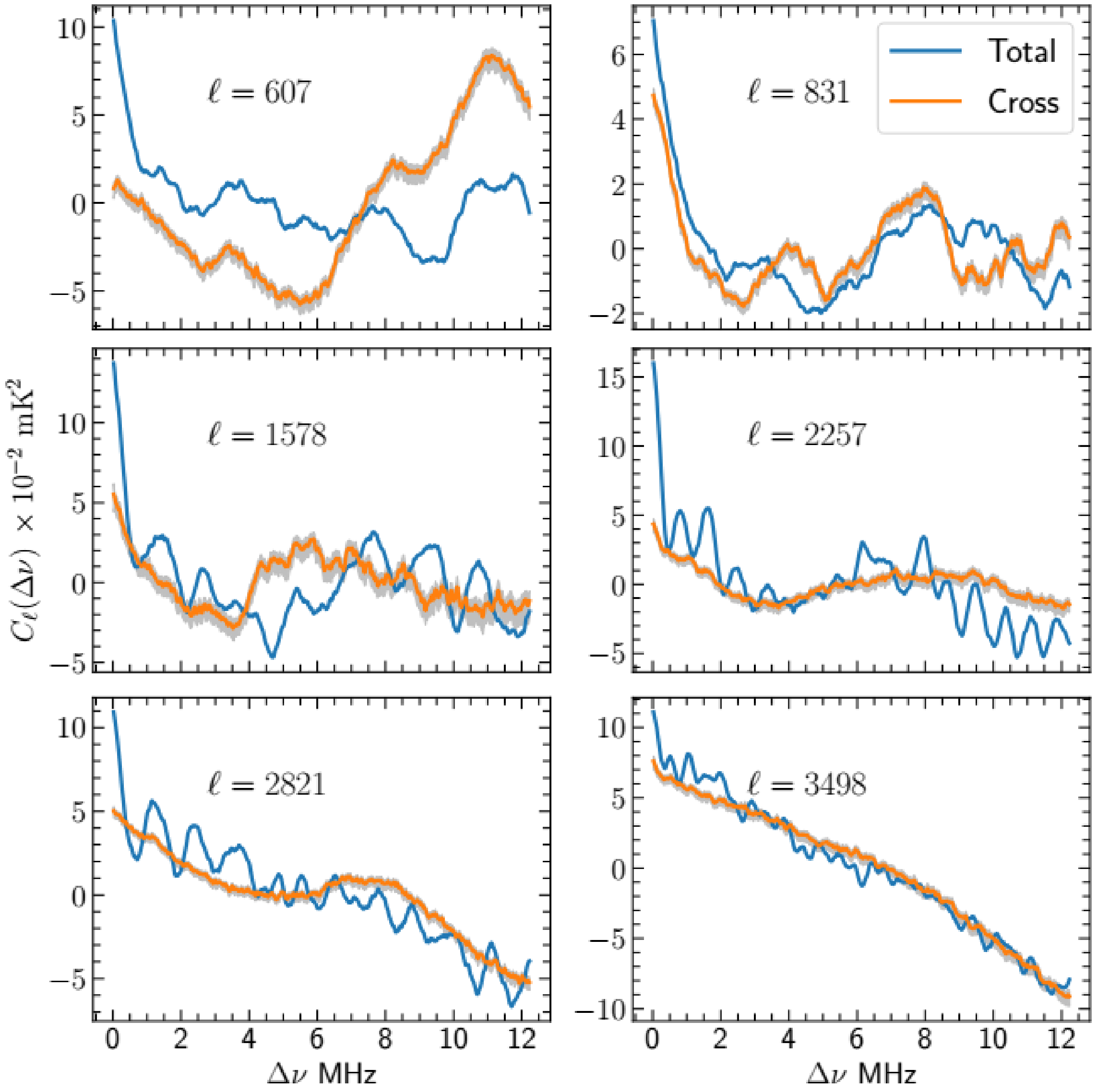


**Figure 2.** A comparison of mean-subtracted Total (blue) and Cross (orange) MAPS $C_\ell(\Delta\nu)$ for different $\ell$-values. The grey shaded regions show the $3\sigma$ error bars.

# Cylindrical PS

Total

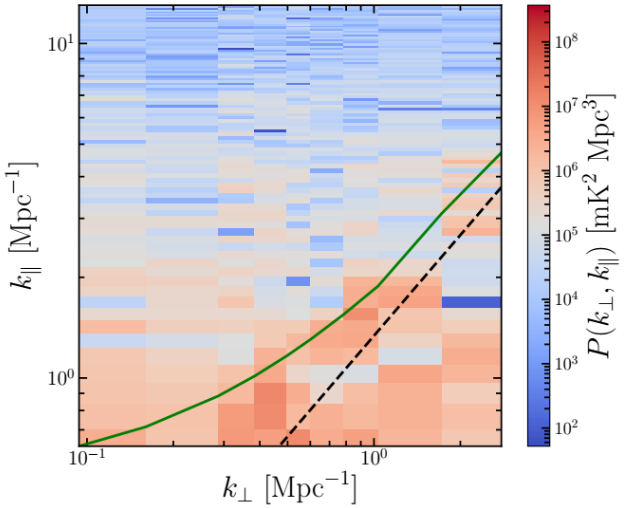


**Figure 9.** The cylindrical power spectra $| P(k_\perp, k_\parallel) |$ for the combined nights data for $f = 0.6$. Here the black-dashed line denotes $[k_\parallel]_H$. The region above the green solid line has been used for spherical binning.

Cross

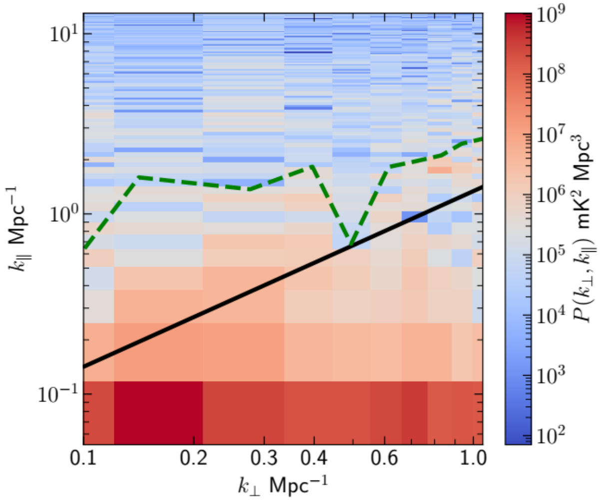


**Figure 4.** The Cross cylindrical power spectra $| P(k_\perp, k_\parallel) |$. Here the black solid and green dashed lines denote $[k_\parallel]_H$ and the TW boundary respectively. The region above the green dashed line was identified as being relatively free of foreground contamination, and used for spherical binning.

t distribution

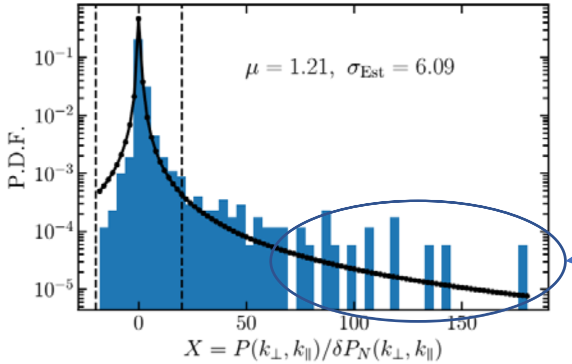


Some Foregrounds still present

Lorentzian distribution

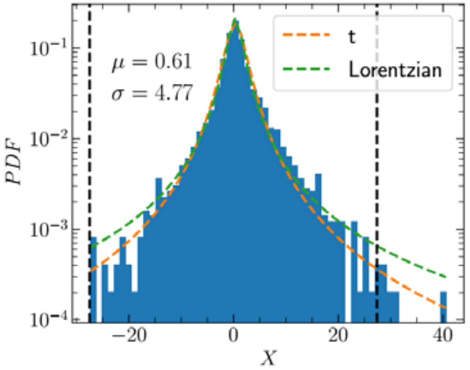

# Foreground Removal

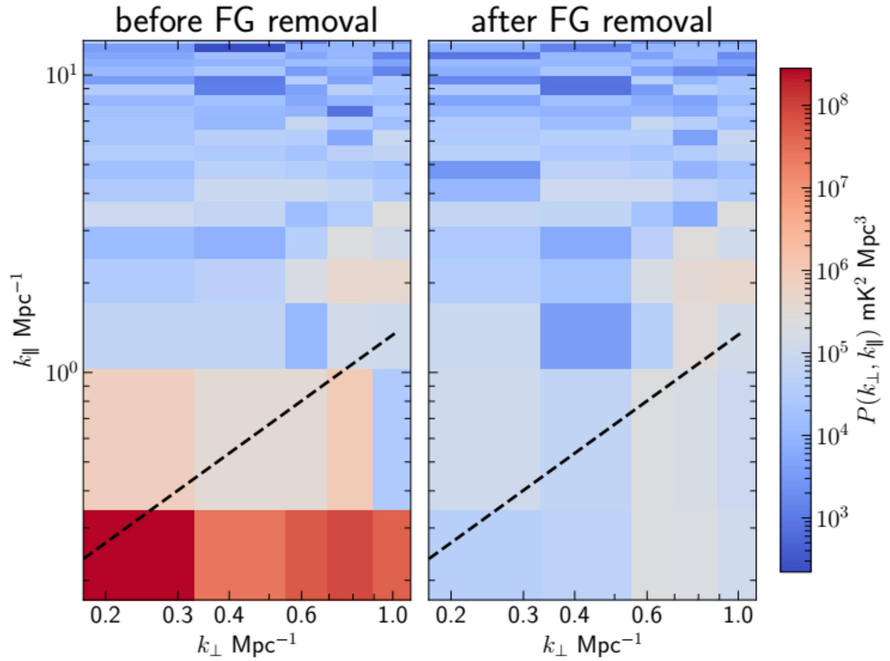


**Figure 4.** The cylindrical PS $\mid P(k_{\perp}, k_{\parallel}) \mid$ before and after foreground removal are shown in the first two panels. The black dashed line shows the theoretically predicted foreground wedge boundary $[k_{\parallel}]_H$.

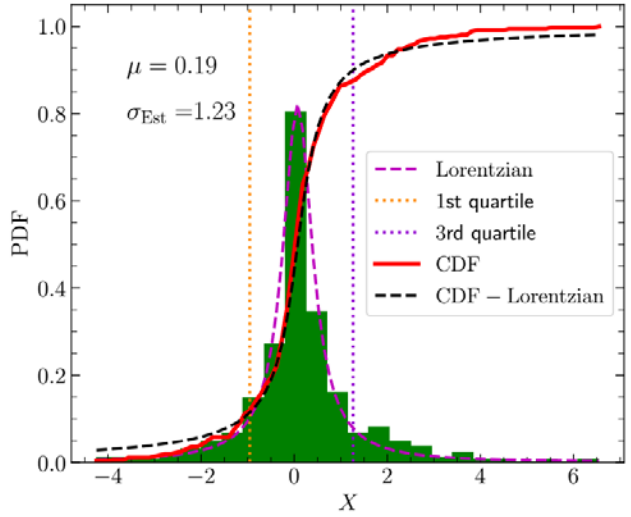


**Figure 5.** The probability density function (PDF) and the cumulative distribution function (CDF) of the variable $X = \frac{P(k_{\perp}, k_{\parallel})}{\delta P_N(k_{\perp}, k_{\parallel})}$ are shown by the green vertical bars and the red solid line, respectively. Lorentzian fits of the PDF and the CDF are shown by the magenta and black dashed lines, respectively. The orange and violet vertical lines show the first and the third quartile of the best-fit Lorentzian distribution. The mean ($\mu$) and the standard deviation ($\sigma$) of $X$ is annotated.

Details in poster by Asif ELahi

Alahi, S. et al. 2023 Submitted

# Spherical PS

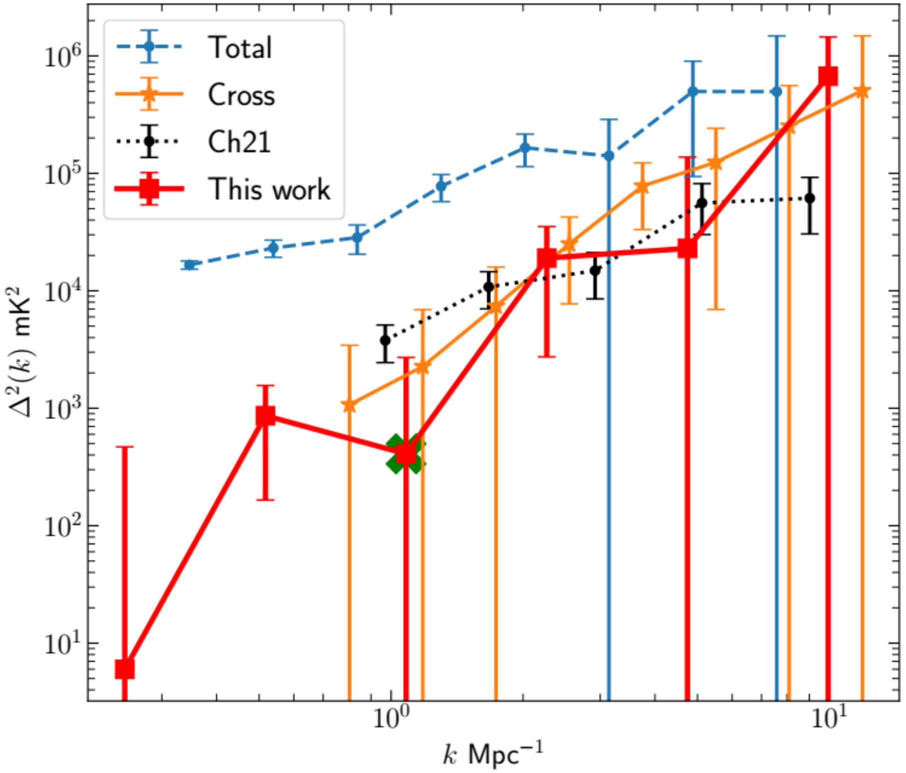


**Figure 6.** The mean squared brightness temperature fluctuations $\Delta^2(k)$ along with $2\sigma$ error bars. The red squares show the results from the present work, whereas the blue, orange and black lines show the results from the Paper I, Paper II and Ch21, respectively.

**Table 2.** The upper limits from 21-cm IM experiments using this uGMRT Band 3 data. The $[\Omega_{\rm H\,I} b_{\rm H\,I}]_{UL}$ values quoted inside the parentheses (...) are obtained when a single, $k$-independent, value of $[\Omega_{\rm H\,I} b_{\rm H\,I}]$ is directly constrained from $C_\ell(\Delta\nu)$ (Section 6).

| Works | $z$ | k Mpc$^{-1}$ | $[\Delta^2(k)]_{UL}$ mK$^2$ | $[\Omega_{\rm H\,I} b_{\rm H\,I}]_{UL}$ |
|---|---|---|---|---|
| Ch21 | 1.96 | 0.99 | $(58.57)^2$ | 0.09 |
| | 2.19 | 0.97 | $(61.49)^2$ | 0.11 |
| | 2.62 | 0.95 | $(60.89)^2$ | 0.12 |
| | 3.58 | 0.99 | $(105.85)^2$ | 0.24 |
| Paper I | 2.28 | 0.35 | $(133.97)^2$ | 0.23 |
| Paper II | 2.28 | 0.80 | $(58.67)^2$ | 0.072 (0.061) |
| Present work | 2.28 | 0.25 | $(21.66)^2$ | 0.044 (**0.022**) |

Consistent with s sigma noise levels
Approximately ten times larger than predicted signal

Alahi, S. et al. 2023 (in preparation)

# Summary

- Tapered Gridded Estimator – 2 steps
- MAPS -> PS
- Tapers Widefield and Sidelobe response
- Missing Channels (Flagging)
- 150 MHz GMRT data
- 420 MHz uGMRT data
- Foreground Removal
- Future: Wideband estimator (~100 MHz) for MAPS

Thank you

# 150 MHz GMRT Observations (2008)

**Table 1.** Observation summary

| | |
|---|---|
| Central Frequency ($\nu_c$) | 153 MHz |
| Channel width ($\Delta\nu_c$) | 62.5 kHz |
| Bandwidth ($B_{bw}$) | 8.00 MHz |
| Total observation time | 11 hrs |
| Target field $(\alpha, \delta)_{2000}$ | ($05^h30^m00^s$, $+60°00'00''$) |
| Galactic coordinates ($l, b$) | 151.80°, 13.89° |
| Off source noise | 1.3 mJy/Beam |
| Flux density (max., min.) | (905 mJy/Beam, −14 mJy/Beam) |
| Synthesized beam | $21'' \times 18''$ , PA = 61° |
| Comoving distance at 153 MHz ($r$) | 9231 Mpc |
| $r'$ at 153 MHz ($dr/d\nu$) | 16.99 Mpc/MHz |

| Angular resolution | rms (mJy/Beam) | Conversion factor (mJy/Beam) to (K) | rms (K) |
|---|---|---|---|
| $620'' \times 540''$ | 23.50 | 0.17 | 4.00 |

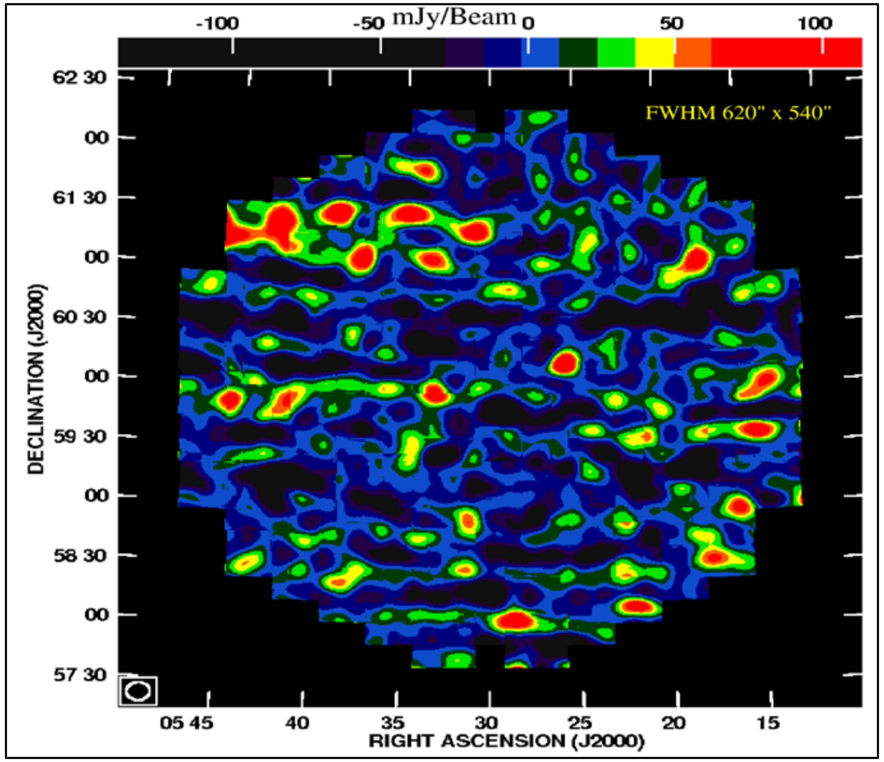


Sources > 9 mJy removed

Ghosh et al. 2012